Polymer 53 (2012) 2964–2972

Contents lists available at SciVerse ScienceDirect

Polymer

journal homepage: www.elsevier.com/locate/polymer

Phthalimide based polymers of intrinsic microporosity

Saad Makhseed*, Fadi Ibrahim, Jacob Samuel

Department of Chemistry, Kuwait University, P.O. Box 5969, Safat 13060, Kuwait

ARTICLE INFO

Article history:
Received 29 December 2011
Received in revised form
18 April 2012
Accepted 2 May 2012
Available online 10 May 2012

Keywords:
Microporous polymers
Membrane
Molecular weight distribution

ABSTRACT

A series of phthalimide based microporous polymers were successfully prepared by conventional nucleophilic substitution reaction of several newly synthesized fluoro-monomers with commercially available 5,5′,6,6′-tetrahydroxy-3,3,3′,3′-tetramethylspirobisindane. FTIR, ^{1}H NMR, and elemental analyses were used to identify the proposed structures of the polymers. The synthesized polymers are of high molecular weight as demonstrated by Gel Permeation Chromatography (GPC). Thermogravimetric analysis shows that the prepared polymers were stable up to 300 °C. From the porosity analysis it is clear that the prepared polymers are analogous to polymers of intrinsic microporosity (PIMs) with high surface area (500–900 m^2/g). The t-plot analysis shown that the major contribution to the specific surface area is arising from the micropore surface area with narrow size distribution of ultramicropores as confirmed by the Horvath-Kawazoe (H-K) analysis. The hydrogen storage capacity of the prepared PIM-R(1–7) and CO-PIM(3,4,6,7) were promising (up to 1.26 wt%, 77 K, at 1.13 bar) with high isoteric heats of H_2 adsorption (8.5 kJ/mol).The results of this study demonstrate that controlling the appropriate monomer content via the three-dimensional structure can provide a uniform microporous morphology in the target polymers.

1. Introduction

The preparation of purely organic microporous polymers without the assistance of molecular template is becoming a fast developing area in nanomaterial's research and many approaches have been used to develop various insoluble network organic microporous polymers such as hyper cross-linked polymers (HCP) [1,2], triptycene-based PIM (Trip-PIM) [3], organic framework polymer (OFP) [4], covalent triazine frameworks (CTFs) [5] and microporous polyimide networks [6] with high specific surface. Conjugated microporous polymers (CMPs) and their analogues are another important class of insoluble microporous organic polymers which can be considered as cross-linked polymers with extended conjugated network [7]. On the other hand, the inclusion of certain functionalities into CMPs can affect their surface areas in comparison with their non-functionalized analogues [8]. Recently many reviews published on nanoporous polymers and their potential applications with a focus on microporosity [9–12]. The microporosity is maintained by a robust network of covalent bonds, further complemented by rigid framework structure. Generally non-network polymers can pack space efficiently leading to nonporous material. It is important to note that if there is a certain amount of free volume, voids would be interconnected, and the polymer will therefore behave as a microporous material even without a network structure. This kind of microporous polymer could be soluble to facilitate easy solution-based processing which can't be achieved in other microporous materials. As a result they have attracted good acceptance as outstanding membrane in gas separation, gas storage, adsorption of small molecules and heterogeneous catalysis [13]. So it is of great interest to synthesize highly soluble porous polymers using the established dioxane-forming polymerization reaction between appropriate fluorine-containing monomers and the commercially available aromatic tetrol. The porous properties mainly due to the architectural features of the used monomers which defines the microporosity. The combined features: high rigidity arising from dioxane linkages and the randomly contorted structure due to either a spiro-centre or a non-planar architecture, represent a prerequisite to induce space inefficient packing producing a large amount of interconnected free volume. The most outstanding representation for this kind of materials are the polymers of intrinsic microporosity (PIMs) [14] developed by McKeown et al with high surface areas in the range of 500–900 m^2/g. Typical example is PIM-1, prepared as a soluble polymer by the dioxane-forming reaction between 5,5′,6,6′-tetrahydroxy-3,3,3′,3′-tetramethylspirobisindane and tetrafluoroterephthalonitrile. The same concept of using rigid

---

* Corresponding author. Tel.: +965 24985538; fax: +965 24816482.
E-mail address: saad.makhseed@ku.edu.kw (S. Makhseed).

0032-3861/$ – see front matter © 2012 Elsevier Ltd. All rights reserved.
doi:10.1016/j.polymer.2012.05.001

and space inefficient packing subunits was expanded by Guiver et al. in developing a high molecular weight PIM-1; synthesized by polycondensation under high-intensity mixing conditions at about 155 °C to yield cyclic-free products in a shorter time (8 min) [15]. McKeown et al, additionally synthesized a highly soluble microporous polymer derived from Bis(phenazyl) monomers with reasonable internal surface area and good film-forming characteristics (PIM-7) [16]. Studies on evaluating the influence of intermolecular interactions in microporous polymers shown that such interactions (e.g. hydrogen bonding) can lead to hindered or reduced microporosity [17,18]. The structural features of PIM-1 further tailored by post- polymerization modifications through the conversion of nitrile moieties into different functional groups such as tetra azole and thioamide with enhanced CO_2 capture and gas transport properties [19,20]. To date, several soluble ladder polymers such as polybenzodioxanes, polyimides, and PIMs containing dinaphtyl or tianthrene segments have been reported and the influence of their modified chemical structure on the physical properties, sorption behaviour and gas permeability has been explored [21–23]. Although the structural alteration of PIM-1 led to low surface areas, these materials showed promising results for certain applications [24].

Controlling the pore diameter at the micro scale (IUPAC pores of dimension < 2 nm) make it possible to use such materials in different commercial applications such as hydrogen adsorption [13]. The lack of fundamental understanding of interaction between the polymer surfaces and the gas molecules initiate many approaches with the aim of designing polymer materials to establish the structure-porous property relationship. This may be achieved by selecting appropriate monomer precursors with certain structural features. For example, monomers decorated by larger substituents can frustrate the resulting polymer chain packing which may create higher surface area along with tunable porosity. In the present study we described a series of solution processable phthalimide based organic polymers prepared from inexpensive monomers with sufficient surface area and narrow pore diameter distribution to store H_2 in the confined space through enhanced interaction. While considering hydrogen storage application the prepared microporous polymers (PIM-Rs and CO-PIM-Rs) offer many attractive features such as low intrinsic density, structural homogeneity, hydrothermal stability and synthetic reproducibility. The chemical features of the surfaces and nature of the pores have thus tuned to achieve a high hydrogen adsorption.

2. Experimental

2.1. Characterization

^{1}H- NMR spectrum (400 MHz) of monomers and polymers were recorded on a Bruker DPX 400 spectrometer using $CDCl_3$ as the solvent and tetramethylsilane as the internal standard. FTIR spectra were recorded on a JASCO FT/IR-6300. Elemental analyses were carried out using Elementar Vario Micro Cube. Mass analyses were done on a Thermo DFS Mass spectrometer. The molecular weight and its distribution were measured by Knauer Gel Permeation Chromatograph fitted with a refractive index detector (flow rate 1 mL/min) according to polystyrene standards using $CHCl_3$ as the eluent. Thermogravimetric analysis (TGA) was performed with a Shimadzu TGA-50 instrument at a heating rate of 10 °C/min under nitrogen atmosphere and DSC analysis was done on Shimadzu DSC-60 instrument at a heating rate of 10 °C/min under nitrogen. Melting points were measured with a Griffin melting point apparatus and further confirmed by DSC analysis. Wide-angle X-ray diffraction (WAXD) of films was measured by a Siemens D5000 diffractometer. Microscopic techniques employed are Scanning Electron Microscopy (SEM: JEOL Model 6300) and High Resolution Transmission Electron Microscopy (HRTEM: JEOL Model JEM-3010). Nitrogen adsorption measurements (77 K) and volumetric hydrogen adsorptions analysis (77 K and 87 K at 1.13 bar) were performed on a Micromeritics ASAP 2020 Sorptometer equipped with an out gassing platform, an online data acquisition and handling system. Before analysis the samples were degassed for 12 h with a heating rate of 1 °C/min in two stages (80 °C for 1 h and 120 °C for 11 h) under high vacuum ($<10^{-4}$ mbar). The specific surface area was calculated using the Brunauer-Emmet-Teller (BET) equation (See supporting Information). The micropore area was calculated using t-plot method (Harkins and Jura). The pore size distributions were calculated from the adsorption isotherm using the Horvath-Kawazoe (H-K) calculations (See supporting Information). The heats of adsorption were calculated from the hydrogen adsorption isotherms obtained at 77.3 K and 87 K using the ASAP 2020 software (Micromeritics, Norcross, GA).

2.2. Materials

The anhydrous solvents DMF and DMAc were purchased from Aldrich co, and the potassium carbonate obtained from Merck was finely grounded and dried at 200 °C. Tetrafluoroterephthalonitrile obtained from aldrich was used directly. 5,5′,6,6′-tetrahydroxy-3,3,3′,3′-tetramethyl-1,1′-spirobisindane obtained from alfa was purified from methanol. Starting from tetrafluorophthalic acid, tetrafluorophthalic anhydride was prepared in our laboratory. The other commercially available materials and solvents were used without further purification.

2.3. Film preparation

Polymer (550 mg) was dissolved in $CHCl_3$ (15 mL) and filtered (2 μm glass microfiber). The filtered solution was pouring into a flat Petri dish (12 cm dia.) and then placed in a vacuum desiccator with the gas inlet open to the atmosphere. The solution was allowed to evaporate for 4 days. The dish was removed and the clear yellow film released from the glass.

2.4. Synthesis of fluoro-monomers

2.4.1. 4,5,6,7-Tetrafluoro-2-phenyl-isoindole-1,3-dione. MR1

Tetrafluorophthalic anhydride (8.5g, 38.7 mmol) was added to a stirred solution of aniline (3.00 g, 32.26 mmol) in glacial acetic acid and refluxed for 12 h. The white solid obtained was further refluxed in acetic anhydride for 12 h. After cooling to room temperature, the precipitated product was filtered off and washed with petroleum ether to give a light yellow solid. Yield: 84%; M_p 206 °C. ^{1}H NMR ($CDCl_3$, δ ppm): 7.26-7.54 (m, 4H, Ar). FTIR (KBr pellet, cm^{-1}): 3068, 1783 (asymmetry C=O), 1726 (symmetry C=O), 1460 (C=C), 1371 (C-N), 945 (C-F). Anal. Calcd for $C_{14}H_5NO_2F_4$ (295.08): C, 56.94; H, 4.74; N, 4.74. Found: C, 56,88; H, 1.80; N, 5.03. MS (EI): m/z (%) 295 (100%).

The following monomers were prepared from tetrafluorophthalic anhydride and corresponding amines using similar procedures adopted for MR1.

2.4.2. 4,5,6,7-Tetrafluoro-2-hexyl-isoindole-1,3-dione. M-R2

Yield: 88%; M_p 118 °C. ^{1}H NMR ($CDCl_3$, δ ppm): 3.68 (t, 2H, CH_2), 1.63-1.70 (m, 2H, CH_2), 1.29-1.35 (m, 6H, CH_2), 0.9 (t, 3H, CH_3). FTIR (KBr pellet, cm^{-1}): 3078, 1780 (asymmetry C=O), 1720 (symmetry C=O), 1465 (C=C), 1370 (C-N), 944 (C-F). Anal. Calcd for $C_{14}H_{13}NO_2F_4$ (303.26): C, 55.45; H, 4.32; N, 4.62. Found: C, 54.70; H, 4.01; N, 4.84. MS (EI): m/z (%) 303 (100%).

2.4.3. 4,5,6,7-Tetrafluoro-2-(4-methoxy-phenyl)-isoindole-1,3-dione. M-R3

Yield: 85%; M_p 250 °C. ^{1}H NMR ($CDCl_3$, δ ppm): 7.28- 7.24 (dd, 2H, Ar), 7.06-7.02 (dd, 2H, Ar), 3.85 (s, 3H, CH_3). FTIR (KBr pellet, cm^{-1}): 3070, 2930, 1775 (asymmetry C=O), 1730 (symmetry C=O), 1468 (C=C), 1338 (C-N), 952 (C-F). Anal. Calcd for $C_{15}H_7$ NO_3F_4 (325.03): C, 55.40; H, 2.17; N, 4.31. Found: C, 55.50; H, 2.07; N, 4.43. MS (EI): *m*/*z* (%) 325 (100%).

2.4.4. 4,5,6,7-Tetrafluoro-2-trimethoxybenzene-isoindole-1,3-dione. M-R4

Yield: 87%; M_p 217 °C. ^{1}H NMR ($CDCl_3$, δ ppm): 6.61 (s, 2H, Ar), 3.91 (s, 3H, CH_3), 3.88 (s, 6H, CH_3). FTIR (KBr pellet, cm^{-1}): 3087, 2935, 1760 (asymmetry C=O), 1728 (symmetry C=O), 1462 (C=C), 1350 (C-N), 960 (C-F). Anal. Calcd for $C_{17}H_{11}NO_5F_4$ (385.10): C, 52.98; H, 2.89; N, 3.64. Found: C, 52.58; H, 2.88; N, 3.85. MS (EI): *m*/*z* (%) 385 (100%).

2.4.5. 4,5,6,7-Tetrafluoro-2- 4-tert -butylbenzene − isoindole-1,3-dione. M-R5

Yield: 84%; M_p 221 °C. ^{1}H NMR ($CDCl_3$, δ ppm): 7.54–7.51 (dd, 2H, Ar), 7.30–7.28 (dd, 2H, Ar), 1.35 (s, 9H, CH_3). FTIR (KBr pellet, cm^{-1}): 3095, 2950, 1772 (asymmetry C=O), 1735 (symmetry C=O), 1458 (C=C), 1350 (C-N), 960 (C-F). Anal. Calcd for $C_{18}H_{13}NO_2F_4$ (351.1): C, 61.52; H, 3.73; N, 3.98. Found: C, 61.70; H, 3.49; N, 4.17. MS (EI): *m*/*z* (%) 351 (45%).

2.4.6. 4,5,6,7-Tetrafluoro-2-(2,6-diisopropyl-phenyl)-isoindole-1,3-dione. M-R6

Yield: 92%; M_p 171 °C. ^{1}H NMR ($CDCl_3$, δ ppm): 7.48 (t, H, Ar), 7.30-7.28 (d, 2H, Ar), 2.63 (sept, 2H, CH), 1.17-1.16 (d, 12H, CH_3). FTIR (KBr pellet, cm^{-1}): 3090, 2940, 1770 (asymmetry C=O), 1733 (symmetry C=O), 1450 (C=C), 1350 (C-N) and 970 (C-F). Anal. Calcd for $C_{20}H_{17}NO_2F_4$ (379.10): C, 63.30; H, 4.48; N, 3.69. Found: C, 63.12; H, 4.26; N, 3.85. MS (EI): *m*/*z* (%) 379 (50%).

2.4.7. 4,5,6,7-Tetrafluoro -1-adamantylamine. M-R7

Yield: 73%; $M_p > 300$ °C. ^{1}H NMR ($CDCl_3$, δ ppm): 2.44 (s, 6H, CH_2), 2.15 (s, 3H, CH), 1.77-1.74 (d, 3H, CH_2), 1.71-1.68 (d, 3H, CH_2). FTIR (KBr pellet, cm^{-1}): 3103, 2911, 1779 (asymmetry C=O), and 1732 (symmetry C=O), 943 (C-F). Anal. Calcd for $C_{18}H_{15}NO_2F_4$ (353.10): C, 61.17; H, 4.24; N, 3.96. Found C, 60.86; H, 4.40; N, 4.08. MS (EI): *m*/*z* (%) 353 (100%).

2.5. Synthesis of PIM-R(1–7)

2.5.1. PIM-R1

A mixture of monomer MR1 (0.50 g, 1.69 mmol) and spirobiscatechol (0.57 g, 1.69 mmol) in dry DMF (50 ml) and K_2CO_3 (0.50g, 3.51 mmol) was stirred at 120 °C for 4 h. After cooling, the reaction mixture was poured into deionised water and the solid product collected by filtration washed with methanol. The insoluble polymer was then purified by refluxing in methanol and acetone. The obtained yellow fluorescent powder was dried in vacuum oven at 100 °C for 12 h. Yield: 75%. $M_p > 300$ °C. M_w 42,403. M_n 40,152. ^{1}H NMR ($CDCl_3$, 298 K δ ppm): 7.68-7.38 (s, br, 3H, Ar), 6.87-6.51 (d, br, 4H, Ar), 2.30 (d, br, 4H, CH_2), 1.30 (s, br, 12H, CH_3). FTIR (KBr pellet, cm^{-1}): 3088, 1774 and 1723 (imide). Anal. Calcd for $C_{35}H_{25}NO_6$ (555.45): C, 75.61; H, 4.50; N, 2.52. Found: C, 75.19; H, 4.43; N, 2.45.

The following polymers were prepared from corresponding fluoro-monomers using similar procedure adopted for PIM-R1.

2.5.2. PIM-R2

Yield: 82%. $M_p > 300$ °C. M_w 27,624. M_n 15,741. ^{1}H NMR ($CDCl_3$, 298 K, δ ppm): 6.91(s, br, Ar), 6.50 (s, br, Ar), 3.45 (m, br, 2H, CH_2), 2.18 (d, br, 2H, CH_2), 1.58-1.30 (d, br, 12H, CH_3). FTIR (KBr pellet, cm^{-1}): 3080, 2940, 1774 and 1709 (imide). Anal. Calcd for $C_{35}H_{33}NO_6$ (563.01): C, 74.60; H, 5.86; N, 2.04. Found: C, 74.28; H, 5.77; N, 2.01.

2.5.3. PIM-R3

Yield: 84%. $M_p > 300$ °C. M_w 178,843. M_n 62,276. ^{1}H NMR ($CDCl_3$, 298 K, δ ppm): 6.95-6.77 (d br, Ar), 6.5 (s br, Ar), 3.85 (t br, OCH_3), 2.30-2.17 (d, br, CH_2), 2.17 (d, 2H, CH_2), 1.31 (s, 12H, CH_3). FTIR (KBr pellet, cm^{-1}): 3090, 1768 and 1717 (imide). Anal. Calcd for $C_{36}NO_7H_{27}$ (585.07): C, 73.84; H, 4.61; N, 2.39. Found: C, 73.48; H, 4.52; N, 2.26.

2.5.4. PIM-R4

Yield: 84%. $M_p > 300$ °C. M_w 214,278. M_n 69,348. ^{1}H NMR ($CDCl_3$, 298 K, δ ppm): 6.89 (s, 2H, Ar), 6.91-6.53 (m br, Ar), 3.90-3.79 (m br, OCH_3), 2.33-2.18 (d, CH_2), 1.72 (s, 2H, CH_2), 1.51(s, 12H, CH_3). FTIR (KBr pellet, cm^{-1}): 1779 and 1712 (imide). Anal. Calcd for $C_{38}H_{31}NO_9$ (645.03): C, 70.69; H, 4.80; N, 2.17. Found: C, 70.57; H, 4.75; N, 2.13.). Anal. Calcd for $C_{38}H_{31}NO_9$ (645.03): C, 70.69; H, 4.80; N, 2.17. Found: C, 70.37; H, 4.71; N, 2.13.

2.5.5. PIM-R5

Yield: 86%; $M_p > 300$ °C. M_w 37,200. M_n 31,000. ^{1}H NMR ($CDCl_3$, 298 K, δ ppm): 7.44-7.31 (d br, Ar), 6.88-6.51 (d br, Ar), 2.30-2.17 (d br, 4H, CH_2), 1.29-1.25 (d, 21H, CH_3). 3086, 2954, 1771 and 1723 (imide). Anal. Calcd for $C_{39}H_{33}NO_6$ (611.24): C, 76.59; H, 5.40; N, 2.29. Found: C, 76.28; H, 5.32; N, 2.21.

2.5.6. PIM-R6

Yield: 87%. $M_p > 300$ °C. M_w 162,594. M_n 67,748. ^{1}H NMR ($CDCl_3$, 298 K, δ ppm): 7.43 (d, 2H, Ar), 6.85 (t br, 2H, Ar), 6.53 (s br, Ar) 2.70(s br, 2H, CH) 2.34-2.09 (d br, 4H, CH_2) 1.32-1.17 (d, 24H, CH_3). FTIR (KBr pellet, cm^{-1}): 3088, 2945, 1781 and 1727 (imide). Anal. Calcd for $C_{41}H_{37}NO_6$ (641.05): C, 76.90; H, 5.75; N, 2.21. Found: C, 76.79; H, 5.68; N, 2.17.

2.5.7. PIM-R7

Yield: 80%. $M_p > 300$ °C. M_w 152,916. M_n 27,803. ^{1}H NMR ($CDCl_3$, 298 K, δ ppm): 6.84-6.72 (d br, 2H, Ar), 6.46 (s br, 2H, Ar), 2.51-2.39 (t br, CH), 2.17-210(d br, 4H CH_2), 1.71-1.67(d br, 12H, CH_2), 1.29 (s br, 12H, CH_3). FTIR (KBr pellet, cm^{-1}): 3098, 2960, 1781 and 1709 (imide). Anal. Calcd for $C_{39}H_{35}NO_6$ (613.08): C, 76.30; H, 5.70; N, 2.28. Found: C, 76.08; H, 5.61; N, 2.19.

2.6. Synthesis of CO-PIM-R(3,4,6,7)

2.6.1. CO- PIM-R3

A mixture of monomer MR3 (0.20g, 0.52 mmol), spirobiscatechol (0.35g, 1.04 mmol) and 2,3,5,6-tetrafluorophthalonitrile (0.10g, 0.52 mmol) in dry DMAc (40 ml) and K_2CO_3 (0.36g, 2.62 mmol) was stirred at 120 °C for 4 h. After cooling, the reaction mixture was poured into deionised water and the solid product collected by filtration and washed with methanol. The insoluble polymer was then purified by refluxing in methanol, acetone and THF. The obtained yellow fluorescent powder was dried in vacuum oven at 100 °C for 12 h. Yield: 85%. $M_p > 300$ °C. M_w 155,908. M_n 125,753. ^{1}H NMR ($CDCl_3$, 298 K, δ ppm): 6.95-6.89 (d br, 2H, Ar), 6.51 (s, 2H, Ar), 3.82 (t br, 3H, OCH_3), 2.30-2.17 (d, 4H, CH_2), 1.31 (s, 12H, CH_3). FTIR (KBr pellet, cm^{-1}): 3070, 2236 (C≡N), 1768 and 1720 imide). Anal. Calcd for $C_{44}H_{37}N_3O_9$ (741.19): C, 71.25; H, 3.67; N, 5.67. Found: C, 70.93; H, 3.52; N, 5.55.

Following copolymers were prepared from corresponding fluoro-monomers using similar procedure adopted for CO- PIM-R3.

2.6.2. CO- PIM-R4

Yield: 80%. $M_p > 300$ °C. M_w 186,930. M_n 148,563. ^{1}H NMR ($CDCl_3$, 298 K, δ ppm): 7.31–7.27 (dd, 2H, Ar), 7.10-7.06 (dd, 2H, Ar), 3.85 (s, 3H, CH_3). FTIR (KBr pellet, cm^{-1}): 3088, 2239(C≡N), 1767 and 1721 (imide). Anal. Calcd for $C_{46}H_{31}N_3O_{11}$ (801.23): C, 68.91; H, 3.90; N, 5.24. Found: C, 68.48; H, 3.74; N, 5.16.

2.6.3. CO-PIM-R6

Yield: 83%. $M_p > 300$ °C. M_w 162,000. M_n 142,000. ^{1}H NMR ($CDCl_3$, 298 K, δ ppm): 7.43–7.28 (d br, 2H, Ar) 6.94-6.90 (d br, 2H, Ar), 6.52-6.44(d br, 2H, Ar), 3.96 (s, 3H, CH_3), 3.80 (s, 6H, CH_3). FTIR (KBr pellet, cm^{-1}): 3090, 2236 (C≡N), 1768, 1721 (imide). Anal. Calcd for $C_{49}H_{37}N_3O_8$ (795.21): C, 73.95; H, 4.69; N, 5.28. Found: C, 73.55; H, 4.41; N, 5.19.

2.6.4. CO- PIM-R7

Yield: 83%. $M_p > 300$ °C. M_w 178,808. M_n 139,788. ^{1}H NMR ($CDCl_3$, 298 K, δ ppm): 6.87 (d br, 2H, Ar), 6.48 (s br, 2H, Ar), 2.54-2.42 (t br, CH), 2.25-2.17(d br, 4H CH_2), 1.73-1.69(d br, 12H, CH_2), 1.32 (s br, 12H, CH_3). FTIR (KBr pellet, cm^{-1}): 3111, 2965, 2236 (C≡N), 1777 and 1731 (imide), Anal. Calcd for $C_{47}H_{35}N_3O_8$ (769.82): C, 73.33; H, 4.58; N, 5.46. Found C, 73.15; H, 4.42; N, 5.34.

3. Results and discussion

The phthalimide based fluorinated monomers (MR [1-7]) were prepared in good yield by the straight forward one step imidisation reaction between tetrafluorophthalic anhydride and different amines in refluxing acetic acid. The proposed structure and purity of the obtained fluorinated monomers were confirmed by routinely spectroscopic techniques as well as elemental analysis. The possibility of the preparation of ladder polymer was confirmed by making model compounds directly from a reaction between 2 M equivalents of di-tertiarybutyl catechol with the different tetraflurophthalimide (See Supporting Information). The reaction product was characterized by mass, ^{1}H NMR, FTIR spectroscopy and elemental analysis confirming that all the four F atoms were replaced by the two benzodioxane units. The highly efficient reaction (yield >90%) promotes the preparation of microporous organic polymers. The polymers (PIM-R[1–7]) were synthesized by the dibenzodioxane formation reaction between the 5,5′,6,6′-tetrahydroxy-3,3,3′,3′-tetramethylspirobisindane (spirobiscatechol), and various fluorine-containing monomers (MR[1–7]) in dry DMF as illustrated in Scheme 1. The polymers were isolated by precipitation in acidified water and the resulting powder samples were purified by refluxing in deionised water, methanol and ethanol respectively followed by reprecipitation in a chloroform/methanol mixture to give yellow fluorescent powder in good yield (>85%) attributed to the efficiency of the polycondensation reaction. The solution processable PIM-Rs can be cast into membrane which can be used as a separation membrane, selectively removing one component either from liquid or gas mixture. According to our previous experiments, we note that the synthesis of PIMs having high molecular weight could be carried out at revised conditions especially elevated temperature and high concentration [25]. After a number of trials, we found that the solvent DMF is significantly compatible with the reaction mixture to a great extent and could achieve high molecular weight linear polymers while compared to DMAc and NMP. We optimized the reaction conditions to get high molecular weight polymers using DMF as a solvent that is significantly well-suited with the monomer salts and the polymers dissolved in the reaction mixture at high concentration conditions. The average molecular masses of prepared polymers were estimated by gel permeation chromatography (GPC) relative to polystyrene standard in $CHCl_3$ (Fig. 1). The data obtained from GPC is listed in Table 1. PIM-R3, PIM-R4 and PIM-R6 with relatively high average molecular weight were obtained. The high molecular weight can be attributed to the good solubility of randomly forming polymers in the reaction mixture. On the other hand, GPC curves (See supporting Information) show shoulder peaks in the low molecular weight region while PIM-R5 with reasonable molecular weight was obtained in a quantitative yield without any shoulder peak. This behaviour can be attributed to the presence of cyclic oligomers as a result of the side reactions. It has been reported that in classic polycondensation reactions of bisphenols and bifluoro aromatics for the production of poly(aryl ethers) that a large amount of macrocyclic oligomers were formed [26,27]. During the first step of the base catalysed reaction, the tetra functional spirobiscatechol reacted with a base to give a number of salt which have low solubility and resulted in the formation of cyclic compounds. The low molecular weight, in the case of PIM-R2, probably caused by either less soluble salts of propagating chains or cyclic oligomer formation. However the reaction rate which depends on the structural features and the reactivity of each monomer also represent another key factor in determining the molecular weight. This clearly indicates that the rate-controlling step in the reaction is the dissolution of the salt. Using the similar procedure adopted for PIM-Rs a series of new copolymers (CO-PIM-R3, CO-PIM-R4, CO-PIM-R6 and CO-PIM-R7) by employing tetrafluoroterephthalonitrile were prepared. After many trial procedures by using different feed ratios of monomers, the

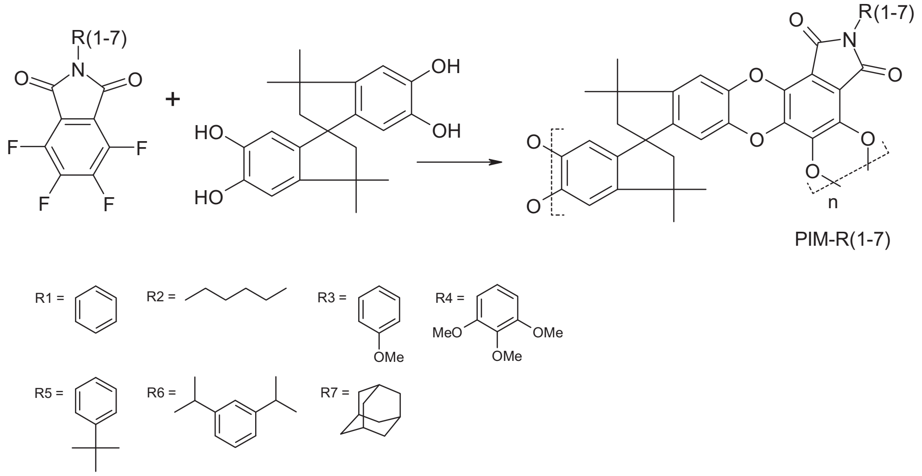

Scheme 1. Synthesis of microporous polymers PIM-R(1–7)s. Reagents and conditions: Dry DMF, Anhydrous K_2CO_3, 120 °C, 4 h.

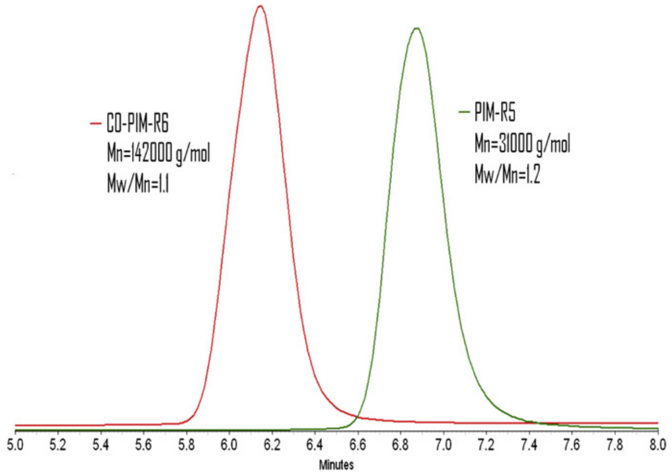

Fig. 1. GPC curves of PIM-R5 and CO-PIM-R6 with narrow molecular weight distribution.

optimum ratio of fluorine-containing monomers and 2,3,5,6-tetrafluorophthalonitrile, which has been applied to produce the maximum molecular weight copolymer is 0.5:0.5. with high molecular weights (M_n; 125,753–148,563). Although the reaction is complicated due to the monomers multiple reactive groups CO-PIM-Rs show GPC curves equivalent to a linear unbranched chain free of macrocyclic species and crosslinking (See Supporting Information). Thus, under the same reaction conditions molecular weight broadening and crosslinking are efficiently reduced by introducing a fixed ratio of tetrafluorophthalonitrile into the reaction mixture, and high-molecular-weight copolymers can be obtained. It is understood that in the reaction mixture tetrafluorophthalonitrile has a higher reactivity, and its polar groups create them active in the reaction system, by the formation of randomly forming the copolymer to a great extent which results in less crosslinking and formation of cyclic oligomers. On the other hand, by using chlorine containing structurally equivalent monomers at different conditions, the high-molecular-weight copolymers still could not be obtained (Scheme 2).

The structures of all PIM-Rs and CO-PIM-Rs were characterized by FTIR, ^{1}H NMR spectroscopy and elemental analysis. All PIMs retained its characteristic stretching bands related to the imide groups (C=O symmetric and asymmetric stretching in the range of 1722–1792). Moreover it is clear from the spectrum that the base catalysed polymerization condition does not make any destruction in the imide units (See Supporting Information). In the ^{1}H NMR spectrum signal positions of PIM-Rs and CO-PIM-Rs were located precisely with the help of ^{1}H NMR spectra of monomers and precursor molecules. The ^{1}H NMR spectra of the PIMs were fully consistent with their proposed structures (See Supporting Information). The signals originating from the hydroxyl groups of spirobiscatechol disappeared, suggesting that the reaction was carried out completely through dibenzodioxane formation. The broad aromatic and aliphatic signals of PIMs were enough to confirm the formation of high molecular weight polymers. The thermal properties were evaluated by TGA and DSC. The decomposition temperatures were also very high; where a 5–10% initial loss around 300 °C, were observed, corresponding to the vaporation of the residual solvents which has been identified as the entrapped solvents in the micropores used for processing the sample (See Supporting Information). The good thermal stability can be attributed to its double stranded structures. In DSC analysis no melting (T_m) and glass transition (T_g) was observed. Wide Angle X-ray Diffraction (WAXD) analysis of the films were conducted to display no crystalline peaks and revealed that all the prepared materials were amorphous. The solubility of the PIM-Rs and CO-PIM-Rs in various organic solvents were tested and found to be highly soluble in $CHCl_3$, and partially in THF, and DMF. The PIMs showed good flexibility, transparency, and the strong thin films could be obtained readily by casting from $CHCl_3$ solutions in all cases (Fig. 2). The mechanical properties of these samples were tested using dumb-bell shaped specimens, except PIM-R2, which did not form a good membrane. As shown in Table 1, tensile strength of all the prepared polymers was comparable irrespective

Table 1
GPC results and mechanical properties of PIM-Rs and CO-PIM-Rs and their comparison with PIM-1.

PIMs	M_n	M_w	M_w/M_n	Tensile strength (MPa)
PIM-1 [14b,23]	96,428	270,000	2.8	47.1
PIM-R1	40,152	42,403	1.27	48.1
PIM-R2	15,741	27,624	1.75	–
PIM-R3	62,276	178,843	2.87	45.0
PIM-R4	69,348	214,278	3.09	46.5
PIM-R5	31,000	37,200	1.20	39.4
PIM-R6	67,748	162,594	2.38	48.6
PIM-R7	27,803	152,916	5.50	41.0
CO-PIM-R3	125,753	155,908	1.24	49.0
CO-PIM-R4	148,563	186,930	1.25	48.4
CO-PIM-R6	142,000	162,000	1.1	48.8
CO-PIM-R7	139,788	178,808	1.27	44.0

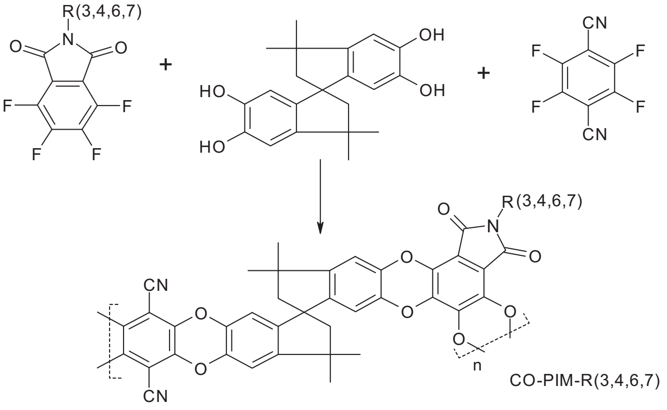

Scheme 2. Synthesis of microporous polymers CO-PIM-R(3,4,6,7). Reagents and conditions: Dry DMF, Anhydrous K_2CO_3, 120 °C, 4 h.

Fig. 2. Transparent free standing PIM-R6 film (M_n = 67748, PDI = 2.38, thickness 70 μm).

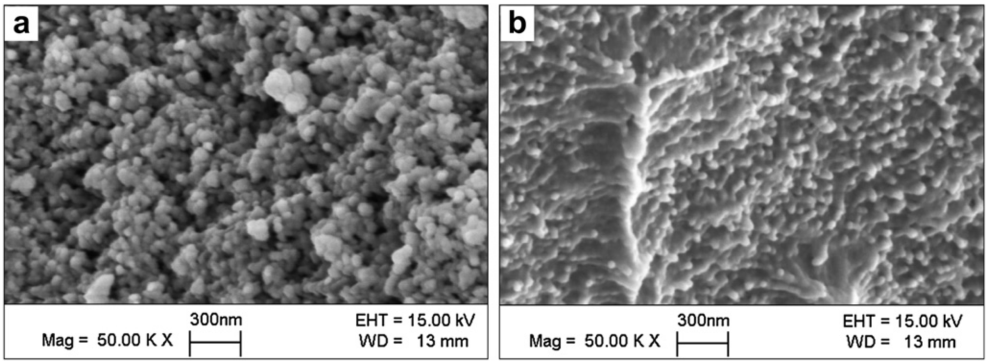

Fig. 3. SEM images of CO-PIM-R6 a) powder and b) thin film.

of their molecular weight. This is attributed to the good structural rigidity due to the presence of strong double stranded backbone (ladder-like sequences). As usually the mechanical properties of linear polymers depend on its molecular weight.

The particle size and morphology of microporous polymers were evaluated by scanning electron microscopy (SEM). Fig. 3 depicts SEM images of the powder and film samples of CO-PIM-R6. The phase homogeneity and uniform size distribution of particles is observed in most of the precipitated samples with considerable differences in surface morphologies of the prepared polymers. The SEM images of the precipitated samples also revealed an aggregation of loosely packed spherically as well as non-spherically shaped micro and nanoparticles (See Supporting Information). The formation of less porous structure in the film can be ascribed to the more densely packed of polymer chains after the solvent evaporation. However the difference in the polymer microstructure due to processing is so significant while considering the sorption ability. Using transmission microscope at high resolution (HRTEM), polymers are seen to have porous structure (Fig. 4). Overall, this is a fairly unique nanoporous structure that dramatically enhances adsorption of small molecules. Like other porous materials (e.g. activated carbons) our prepared polymers were found to be stable under the HRTEM analysis (300 kV) as an additional indication of the high structural stability.

3.1. N_2 sorption analysis

The porous nature of PIMs was analysed by means of nitrogen sorption at 77 K. The most common technique used for screening the porosity involves the fitting of Brunauer-Emmett-Teller (BET) equation to the data obtained from the nitrogen adsorption/desorption isotherms at 77 K. Table 2 lists several relevant parameters obtained from the isotherm analysis including surface areas, micropore area, micropore volume and pore diameter based on Horvath-Kawazoe (H-K). The BET surface areas of PIM-R(1–7)s and CO-PIM-Rs ranged from 500 to 900 m^2/g, with adequate micropore area (438–638 m^2/g). The micropore pore volumes ranging from 0.22 to 0.44 cm^3/g. The difference in specific surface area might be due to the structural geometry of the monomers employed as well as the efficient polycondensation by the incorporation of highly reactive fluorinated monomers into the reaction mixture, resulting in high-molecular-weight copolymers. When comparing the porous properties PIM-Rs and CO-PIM-Rs which are built up from different monomers and comonomers, a trend linking porosity and the comonomer unit can be seen. Typical example of nitrogen adsorption/desorption isotherm is shown in Fig. 5. The adsorption isotherms show high uptake at very low relative pressure, which is characteristic of a microporous material and isotherms of the prepared polymers exhibit a combination of I and II N_2 sorption isotherm with a continuous increase after the adsorption at low relative pressure and a broad hysteresis upon desorption. Suggesting that, a broad hysteresis down to low pressure is indicative of trapping effect at cryogenic temperature. The extremely low relative pressure portion of the adsorption isotherm is related to the apparent micropore distribution, which in turn is expected to have a profound influence on the transport properties of the polymer. From the t-plot analysis it was found that all the prepared polymers showed significant amount of microporosity. Surface area for CO-PIM-Rs found to be higher than its related

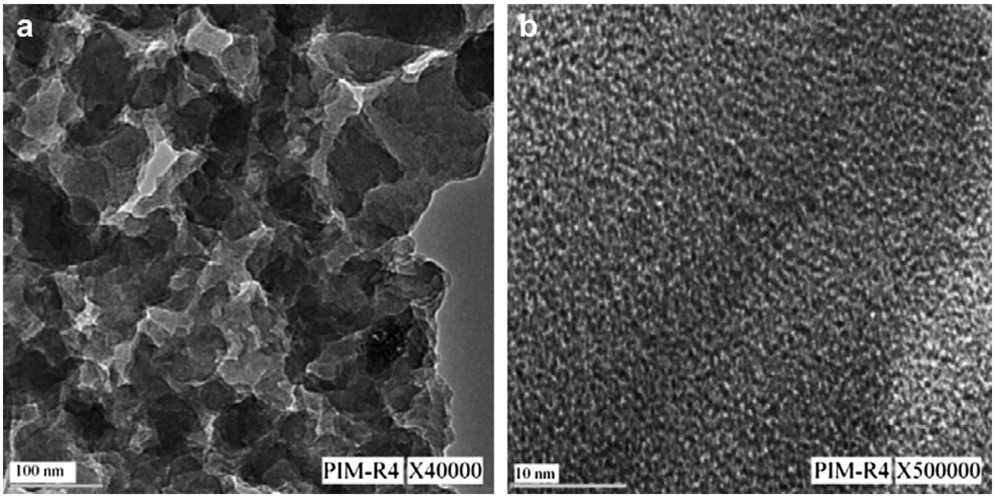

Fig. 4. HRTEM images of PIM-R4 powder at different magnifications.

Table 2
Porous properties of PIM-Rs and CO-PIM-Rs and their comparison with PIM-1 and OFP-3.

PIMs	SA_{BET} (m^2/g)[a]	PV_{micro} (cm^3/g)	HK median pore width (Å)	SA_{LAN} (m^2/g)[b] (77 K/87 K)	H_2 (wt.%)/1.13 bar, (77 K/87 K)	Q_{st} (kJ/mole)
PIM-1 [14b]	860	–	6–7	–	1.04	–
OFP-3 [4]	1159 (1089)	0.69	5–6	934/801	1.56/1.36	7.45
PIM-R1	702 (575)	0.28	7.5	432/323	1.01/0.76	7.24
PIM-R2	595 (548)	0.25	6.6	343/275	0.79/0.63	7.35
PIM-R3	628 (467)	0.23	8.2	467/353	0.97/0.74	7.14
PIM-R4	889 (717)	0.37	7.6	531/436	1.18/0.92	6.85
PIM-R5	636 (457)	0.23	8.3	422/315	0.86/0.63	6.66
PIM-R6	714 (632)	0.32	6.9	453/326	1.03/0.87	7.24
PIM-R7	680 (638)	0.33	6.8	440/346	0.92/0.81	7.37
CO-PIM-R3	843 (813)	0.41	6.6	502/406	1.08/0.92	6.60
CO-PIM-R4	880 (840)	0.42	6.5	545/451	1.26/0.95	7.54
CO-PIM-R6	855 (789)	0.44	6.7	541/422	1.21/0.96	8.55
CO-PIM-R7	857 (549)	0.37	7.8	553/443	1.17/0.91	7.37

[a] BET surface area calculated from nitrogen adsorption isotherm. The number in the parenthesis is the micropore surface area calculated using the t-plot analysis. PV_{micro} is the micropore volume.

[b] Surface area calculated from the H_2 adsorption isotherm using Langmuir equation at 77 K and 87 K.

polymer containing the common repeating unit. Analysis of low relative pressure region of the N_2 adsorption isotherm by the Horvath-Kawazoe (H-K) method assuming a slit-pore geometry gives the apparent micropore distributions is given in the inset of Fig. 5. To induce microporosity in a prepared polymer at least one of the monomer contain a site of contortion [28], which in many cases represented by tetrahedral carbon of a spiral core and moreover pore distribution with the majority of micropores populated at width less than 10 Å. Such narrow pore size distribution is advantageous for better interaction with H_2 molecules and there by enhancing the storage capacity. The high surface areas of intrinsically porous polymers can be illustrated by its rigid nonlinear architecture. It is believed that nonlinear polymers can possess large amount of interconnected void space. The presence of these interconnected voids enhances the intrinsic microporosity of the polymer even without the network structure. The spiro centre present in the 5,5′,6,6′-tetrahydroxy-3,3,3,3′-tetramethyl-1,1′-spirobisindane creates the nonlinearity by propagating the polymer chain in three-dimensional irregular fashion producing a polymer chain that can also prevent the dense packing. The dioxane linkage in conjunction with spiro centre forcing perpendicularly arranged aromatic rings creates the conditions of supramolecular control over the molecular structure.

The porous properties of some selected film samples were tested by means of nitrogen adsorption at 77 K. As expected the measurement were very slow and the film samples showed lower surface area as compared to its powder form, which may be related to the more densely packed structure as confirmed by SEM. Fig. 6 shows the N_2 adsorption/desorption isotherm of CO-PIM-R4 film with a remarkable BET surface area (467 m^2/g). The isotherm displays a considerable uptake at relative low pressure with larger hysteresis due to the swelling/trapping effect [18]. In addition, some film samples show a sudden jump at certain points which can be explained by the getting pressure effect (see supporting information). In comparison to powder samples, all the tested film samples shows same behaviour in the adsorption isotherm which is typical for finely microporous media.

3.2. Hydrogen adsorption

The volumetric hydrogen adsorption capacities of all PIMs were measured using a ASAP 2020 instrument with 99.999% pure H_2 over the pressure range 0–1.13 bar. The sorption of hydrogen at cryogenic temperature is also an important tool to identify the microporosity in polymers. Fig. 7 shows the adsorption/desorption isotherms at 77 and 87 K for the CO-PIM-R4 with a maximum hydrogen adsorption capacities up to 1.24 and 0.96 wt% respectively at 1.12 bar. The isotherms are fully reversible and exhibit a sharp rise at low pressure region which is consistent with the physisorption of hydrogen on a microporous material. All the prepared PIM-Rs and CO-PIM-Rs show similar behaviour in their isotherm with a significant uptake at two different temperatures (Table 2). From the isotherms it was found that there was no kinetic trapping of hydrogen in small pores upon desorption. The Hydrogen adsorption capacities by various samples with different surface areas usually reveal a linear relationship between BET surface area and H_2 storage capacity at low pressure. For example the H_2 adsorption capacity of PIM-R2 (0.79 wt.%) and PIM-R4 (1.18 wt.%) at 1 bar and 77 K with their BET surface areas 595 and 889 m^2/g respectively, is consistent with the above hypothesis. Thus from the comparison of various synthesised PIM-Rs and CO-PIM-Rs, the H_2 adsorption capacities are largely influenced by BET surface area. Several studies showed that a clear relationship exists between total surface area and hydrogen adsorption density of a porous material [29–31]. The hydrogen adsorption at 77 K, physisorption mechanism is dominant and the H_2 uptake is controlled by the structural features of the adsorbent material. Moreover small micropores can effectively adsorb hydrogen, probably due to its much smaller kinetic diameter compared to bigger gas molecules such as N_2 [2b,32]. These ultramicropores allow the dihydrogen molecule to interact with multiple portions of

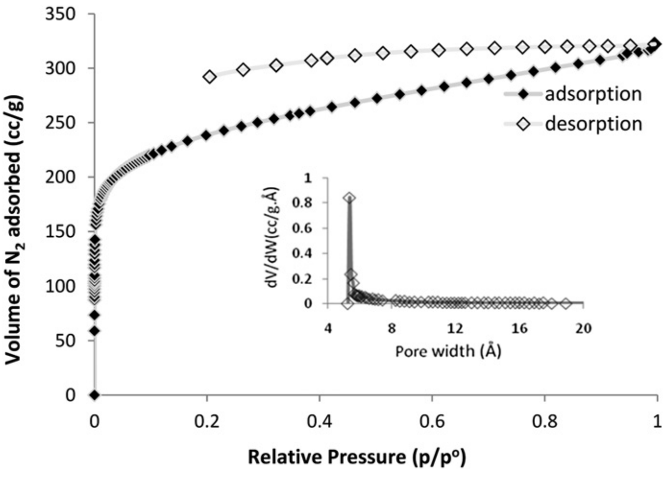

Fig. 5. Nitrogen sorption isotherm of CO-PIM-R4 at 77 K and the inset picture is micropore size distribution as calculated using HK method.

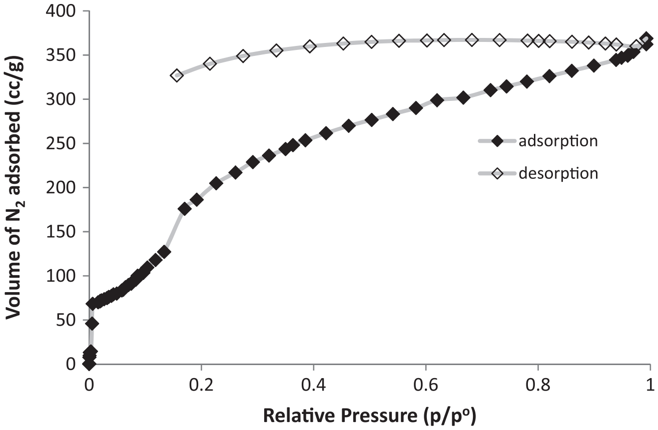

Fig. 6. Nitrogen sorption isotherm of CO-PIM-R4 film at 77 K.

the double stranded framework and thereby increasing adsorption potential and a stronger van der Waals interaction with the hydrogen molecules [33,34]. It is therefore clear that the hydrogen storage capacity is generally relative to their respective specific surface areas as well the presence of ultramicroporosity. The langmuir model is frequently used to measure specific surface area of microporous polymers from hydrogen sorption isotherms and the values ranging upto 550 m^2/g as depicted in Table 2. The Langmuir isotherm theory assumes monolayer coverage of adsorbate over a homogenous adsorbent surface of equal energy. The isosteric heat of adsorption, (Q_{st}), for dihydrogen molecules on all samples was calculated from the adsorption isotherms at 77 and 87 K as shown in Fig. 7. The calculated Q_{st} values (6.6–8.5 kJ/mol) are comparable with other porous organic materials such as COFs, PAFs and HCPs. The highest heat of sorption (8.5 kJ/mol) was observed for CO-PIM-R6indicating a favourable interactions between dihydrogen and polymer surface. As shown in typical example in Fig. 8 the values of Q_{st} decreases rapidly as the function of degree of coverage. This is attributed to the heterogeneous nature of polymer surface (sorption places are energetically different) which is available for adsorption [2]. The chemical nature of the accessable surfaces and morphology of the pores have thus to be tuned to enable a high adsorption enthalpy. It has been already known that microstructure had a deep impact on hydrogen uptake which is further influenced by the geometry of the building units.

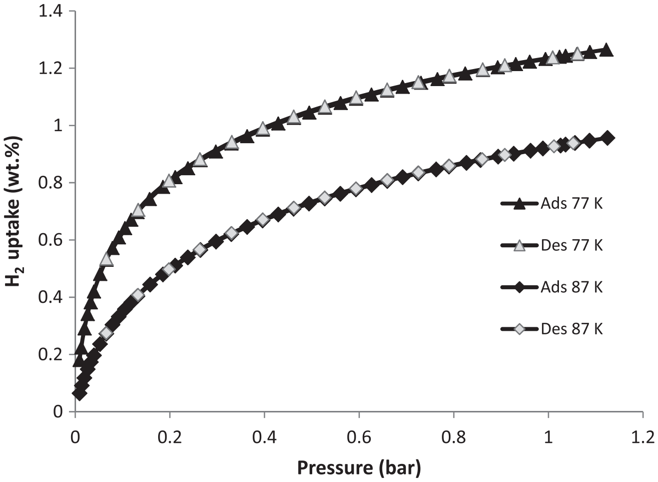

Fig. 7. Hydrogen sorption isotherms of CO-PIM-R4 at 77 K and 87 K.

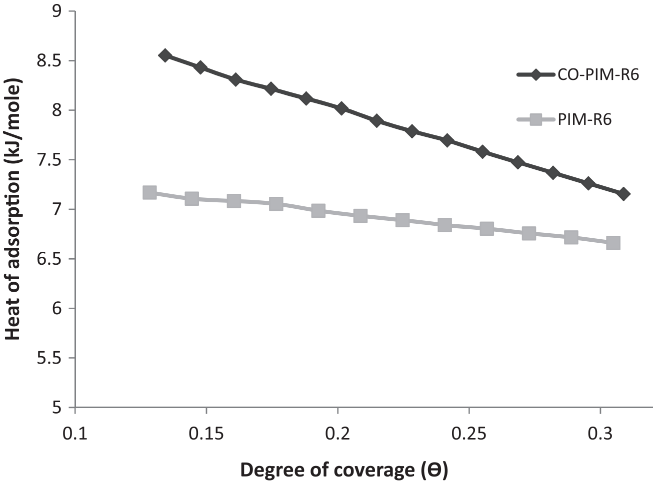

Fig. 8. Isosteric heats of adsorption for H_2 on PIM-R6 and CO-PIM-R6.

In a recent study based on FTIR spectroscopy revealed that the dihydrogen molecules adsorb perpendicular to the surface, the preferential adsorption site is benzene rings [35]. So materials containing high electron rich sites were found to increase the hydrogen adsorption enthalpy. The combination of microporosity and chemical functionality of these PIMs are very promising for applications in the air purification, or separation. As compared to MOFs and similar metal containing porous structures, the concept of preparing hydro-thermally stable PIMs having organic spacers along with predefined functionality allows them to extend in many adsorption applications.

4. Conclusions

In conclusion, a new series of soluble phthalimide based organic polymers exhibiting intrinsic microporosity were synthesized by the nucleophilic substitution reaction using various fluoromonomers and 5,5′,6, 6′-Tetrahydroxy-3,3,3′,3′-tetramethylspirobisindane. The resulting ladder polymers were obtained in high yield. The FTIR, ^{1}H NMR, and elemental analyses indicated that the polymers appear to have the same proposed structure. Reaction conditions led to high molecular weight polymers which provided surface areas up to 900 $m^2\ g^{-1}$. The pore size distribution analysis shown that pores are narrowly distributed and fine-tuned with a subnanometer dimension, close to the van der Waals diameters of various small gas molecules. The intrinsic microporosity of these polymers is supported by good hydrogen uptake at 77 K and 87 K. Isosteric heat of H_2 adsorption (Q_{st}) measurement revealed that Q_{st} is not highly sensitive to the structural features and exhibit high isoteric heats of adsorption up to 8.5 kJ/mol.

Acknowledgements

The authors thank Kuwait University for funding (SC03/08) and the technical support of GFS (GS01/01, GS01/05 and GS01/03) and EMU.

Appendix A. Supporting information

Supplementary data related to this article can be found online at doi:10.1016/j.polymer.2012.05.001.

References

[1] (a) Lee J-Y, Wood CD, Bradshaw D, Rosseinky MJ, Cooper AI. Chem Commun; 2006:2670–2;
(b) Wood CD, Tan B, Trewin A, Niu H, Bradshaw D, Rosseinsky MJ, et al. Chem Mater 2007;19:2034–48.
[2] (a) Germain J, Hradil J, Frechet JMJ, Svec F. Chem Mater 2006;18:4430–5;
(b) Germain J, Svec F, Frechet JMJ. Chem Mater 2008;20:7069–76.
[3] Ghanem BS, McKeown NB, Harris KDM, Pan Z, Budd PM, Butler A, et al. Chem Commun; 2007:67–9.
[4] Makhseed S, Samuel J. Chem Commun; 2008:4342–4.
[5] (a) Kuhn P, Antonietti M, Thomas A. Angew Chem Int Ed 2008;47:3450–3;
(b) Kuhn P, Forget A, Su DS, Thomas A, Antonietti MJ. Am Chem Soc 2008;130:13333–7.
[6] Wang Z, Zhang B, Yu H, Sun L, Jiao C, Liu W. Chem Commun 2010;46:7730–2.
[7] (a) Jiang JX, Su F, Trewin A, Wood CD, Campbell NL, Niu H, et al. Angew Chem Int Ed 2007;46:8574–8;
(b) Jiang JX, Su F, Trewin A, Wood CD, Campbell NL, Niu H, et al. J Am Chem Soc 2008;130:7710–20.
[8] Dawson R, Laybourn A, Clowes R, Khimyak YZ, Adams DJ, Cooper AI. Macromolecules 2009;42:8809–16.
[9] Dawson R, Cooper AI, Adams DJ. Prog Polym Sci 2012;37:530–63.
[10] Thomas A. Angew Chem Int Ed 2010;49:8328–44.
[11] Cooper AI. Adv Mater 2009;21:1291–5.
[12] McKeown NB, Budd PM. Macromolecules 2010;43:5163.
[13] McKeown NB, Budd PM. Chem Soc Rev 2006;35:675–83.
[14] (a) Budd PM, Ghanem BS, Makhseed S, Mckeown NB, Msayib K, Tattershall CE, et al. Chem Commun 2004;2:230–1;
(b) Budd PM, Elabas ES, Ghanem BS, Makhseed S, McKeown NB, Msayib KJ, et al. Adv Mater 2004;16:456–9;
(c) McKeown NB, Budd PM, Msayib K, Ghanem BS, Kingston HJ, Tattershall CE, et al. Chem A Eur J 2005;11:2610–20.
[15] Du N, Song J, Robertson GP, Pinnau I, Guiver MD. Macromol Rapid Commun 2008;29:783–8.
[16] Ghanem BS, McKeown NB, Budd PM, Fritsch D. Macromolecules 2008;41:1640–6.
[17] (a) Du N, Robertson GP, Pinnau I, Guiver MD. Macromolecules 2009;42:6023–30;
(b) Du N, Robertson GP, Song J, Pinnau I, Guiver MD. Macromolecules 2009;42:6038–43.
[18] Weber J, Du N, Guiver MD. Macromolecules 2011;44:1763–7.
[19] Du N, Park HB, Robertson GP, Dal-Cin MM, Visser T, Scoles L, et al. Nat Mater 2011;10:372–5.
[20] Mason CR, Maynard-Atem L, Al-Harbi NM, Budd PM, Bernardo P, Bazzarelli F, et al. Macromolecules 2011;44:6471–9.
[21] Weber J, Su Q, Antonietti M, Thomas A. Macromol Rapid Commun 2007;28:1871–6.
[22] (a) Ritter N, Antonietti M, Thomas A, Senkovska I, Kaskel S, Weber J. Macromolecules 2009;42:8017–20;
(b) Ritter N, Senkovska I, Kaskel S, Weber J. Macromol Rapid Commun 2011;32:438–43.
[23] Du N, Robertson GP, Pinnau I, Guiver MD. Macromolecules 2010;43:8580–7.
[24] Dawson R, Laybourn A, Khimyak YZ, Adams DJ, Cooper AI. Macromolecules 2010;43:8524–30.
[25] Makhseed S, Samuel J, Bumajdad A, Hassan M. J Appl Polym Sci 2008;109:2591–7.
[26] Kricheldorf HR, Schwarz G. Macromol Rapid Commun 2003;24:359–81.
[27] Miyatake K, Hlil AR, Hay AS. Macromolecules 2001;34:4288.
[28] Carta M, Raftery J, McKeown NB. J Chem Crystallo 2011;41:98–104.
[29] Dinca M, Yu AF, Long JR. J Am Chem Soc 2006;128:17153. 17153.
[30] Foy AGW, Matzger AJ, Yaghi OM. J Am Chem Soc 2006;128:3494–5.
[31] Mckeown NB, Gahnem B, Msayib KJ, Budd PM, Tattershall CE, Mahmood K. Angew Chem Int Ed 2006;45:1804–7.
[32] Weber J, Antonietti M, Thomas A. Macromolecules 2008;41:2880–5.
[33] Shiraishi M, Takenobu T, Yamada A, Ata M, Kataura H. Chem Phys Lett 2002;358:213–8.
[34] Yushin G, Dash RK, Jagiello J, Fischer JE, Gogotsi Y. Adv Funct Mater 2006;16:2288–93.
[35] Spoto G, Vitillo JG, Cocina D, Damin A, Bonino F, Zecchina A. Phys Chem Chem Phys 2007;9:4992–9.